Original Article

Institution of MECHANICAL ENGINEERS
Journal of MECHANICAL ENGINEERING SCIENCE

Proc IMechE Part C:
J Mechanical Engineering Science
0(0) 1–19

DOI: 10.1177/0954406218774362
journals.sagepub.com/home/pic
SAGE

Numerical and experimental nonlinear dynamic response reduction of smart composite curved structure using collocation and non-collocation configuration

Vijay K Singh[1], Chetan K Hirwani[2], Subrata K Panda[3], Trupti R Mahapatra[4] and Kulmani Mehar[2]

Abstract

In this work, a generic geometrical nonlinear mathematical model of smart composite curved shell panels has been developed for the evaluation of the linear and nonlinear dynamic responses. Further, the dynamic deflections are reduced by employing the piezoelectric material with the parent composite using two different arrangements (sensor and actuator). The current layered structure model is developed based on the higher-order mid-plane kinematics including the stretching effect. The electric potential due to the piezoelectric material included via a quadratic function of thickness for the current combined electro-elastic modeling. The geometrical distortion of the smart shell panel structure accounted via Green-Lagrange strain field including all of the nonlinear higher-order terms. The desired responses are evaluated computationally using an original computer code (MATLAB environment) with the help of the current higher-order model and finite element steps. The nonlinear dynamic deflection values are obtained through the direct iterative method in conjunction with Newmark's integration. Additionally, the accuracy of the proposed model is demonstrated via comparison study with the available published literature with and without electric field potential. The reduction of response frequencies is also compared with the in-house experimental data. Lastly, few more numerical examples are computed for the various geometrical parameter including the shell configuration and the comprehensive behaviour of the currently developed nonlinear numerical model for the analysis of smart layered structure discussed in details.

Keywords

Geometrical nonlinearity, higher order shear deformation theory, laminated curved structure, finite element method, polyvinylidene difluoride, active fiber composite, collocated/noncollocated

Date received: 8 October 2017; accepted: 9 April 2018

Introduction

Since last few decades, the multi-layered composite material has been popular and extensively used in various weight-sensitive industries due to light-weight and flexible properties.[1–3] Similarly, the piezoelectric material, due to its electromechanical coupling behaviour is preferably used in sensing and actuating applications. By combining the traditional advantages of the layered composite material with that of the inherent capability (electromechanical coupling behaviour) of piezoelectric material, a hybrid smart composite is developed. Nowadays, the hybrid composite of layered structure embedded with piezoelectric layer or patches, gaining huge attention for potential application in structural health monitoring, shape control and precision positioning, automotive sensing and actuating configuration, vibration and noise suppression in aircraft, aerospace, ship building and similar industries. This is due to their outstanding properties such as flexibility, light-weight,

[1]Department of Mechanical Engineering, Vignan Foundation for Science Technology and Research (VFSTR), Vadlamudi, Guntur, AP, India
[2]Mechanical Engineering Department, National Institute of Technology Rourkela, Rourkela, India
[3]Department of Mechanical Engineering, National Institute of Technology Rourkela, Rourkela, India
[4]Production Engineering Department, VSSUT Burla, Sambalpur, India

Corresponding author:
Subrata K Panda, Department of Mechanical Engineering, National Institute of Technology Rourkela, India.
Email: call2subrat@gmail.com

self-controlling and/or self-monitoring capabilities, wide bandwidth and quick response ability, availability in thin form etc.[4–6] To attain superior design and manufacturing of these structures for the safe application in various areas, it is highly important for the design engineers to envisage the mechanical behaviour accurately prior to the final design. In order to do so various analytical, semi-analytical, numerical and exact solutions for the smart layered composite structure have been provided in the past by many researchers. Few pioneer, related and important works available in the open literature have been reviewed and presented in the following lines.

The piezoelectric laminate theory is proposed by Lee[7] that is capable of replicating the influence of the actuating (electromechanical) and sensing (mechanoelectrical) behaviour of the laminate. Pai et al.[8] developed the refined nonlinear model for the laminate structure embedded with piezoelectric material based on the higher order shear deformation theory (HSDT) and layerwise theory. Mitchell and Reddy[9] introduced a refined hybrid theory for laminated composite with the piezoelectric layer such that the mechanical displacement field and the potential function for piezoelectric laminate are based on the equivalent single layer theory and layerwise theory, respectively.

The finite element method (FEM) is known to be a robust tool for solving more complex engineering problems. Dynamic behaviour of laminated composite embedded with lead zirconate titanate (PZT) patches is analysed by Lee and Ng[10] and Sunar and Al-Bedoor[11] using FEM. The linear and nonlinear dynamic characteristic of laminated composite structure with surface bonded smart material is investigated using the linear and nonlinear FE models based on the first order shear deformation theory (FSDT)[12] and the HSDT[13] in conjunction with layerwise and/or single layer theory approximation. Mateescu et al.[14] investigated the dynamic characteristic of smart damaged structure subjected to aerodynamic loading. In the similar line, the geometrical nonlinear time-dependent mechanical responses of the doubly curved sandwich shell panel embedded with the piezoelectric layer are analysed by Kumar and Ray[15] using nonlinear 3D FE model in conjunction with the FSDT and von Karman nonlinear strain.

Analytical solutions for the nonlinear dynamic response of layered composite plate with piezoelectric material subjected to combined thermo-electro-mechanical loading is presented by Huang and Shen[16] by considering the geometrical nonlinearity in von Karman sense. Similarly, the free and forced vibration responses of the smart layered composite with an acoustic enclosure is provided by Shahraeeni et al.[17] using the classical lamination theory (CLT). Jiang et al.[18] also developed an analytical solution approach by using refined plate theory to analyse the dynamic responses of the piezoelectric laminated plate. Phung-Van et al.[19] obtained the static and dynamic responses of the smart laminated composite structure by developing the mathematical model in the framework of the HSDT using isogeometric analysis (IGA) method. Later, they (Phung-Van et al.[20]) extended the analysis of nonlinear transient responses by developing the nonlinear model using the generalized unconstrained approach in conjunction with IGA and von-Karman type of geometrical nonlinearity. Subsequent development of the mathematical modeling further extended to analyse the plate/shell structures using Carrera Unified Formulation (CUF) with and without considering the effect of the smart materials. In this regard, a significant amount of studies reported[21–25] to handle a large variety of plate/shell models in a unified manner. The studies indicate that CUF theory has a major advantage that it can have an order of expansion which goes from first to higher-order values, and, can be regarded as an equivalent single layer or layer-wise depending on the thickness functions adopted.

Further, the exact solutions of the static deflections of the functionally graded (FG) structure embedded with piezoelectric fiber reinforced composite (PFRC) material are reported by Ray and Sachade.[26] Similarly, the transient behaviour of the layered smart composite structure investigated by Qing et al.[27] via modified mixed variational principle using the propagator matrices method. The flexural vibration of layered cylindrical shell panel with PFRC actuators is analysed by Shen and Yang[28] using HSDT mid-plane kinematics and the geometrical nonlinearity in von Karman sense. Saviz[29] presented the elasticity solution to the dynamic response of cylindrical shell with surface bonded piezoelectric layer by incorporating both the displacement and electric potential field via Legendre polynomial expansion.

From the extensive review, it is noted that various nonlinear mathematical model proposed including the new solution technique to compute the mechanical responses of the smart layered composite structure in the past. However, in most of the studies, we note that von-Karman type of strain–displacement relations utilised for the geometrical nonlinear modeling purpose. It is well known that the geometrical nonlinearity in von-Karman sense does not include all of the nonlinear terms associated with the structural deformation and comprised with the moderate rotations only. For the incorporation of large rotation and distortion, it does not meet the realistic case. Whereas, the nonlinear strain field in Green-Lagrange form is not only accurate but also represent the general configuration of any deformed structure. Also, noted that the limited numbers of the article reported on the nonlinear transient behaviour of the doubly curved laminated shell panel embedded with

the piezoelectric material including the experimental validation for the reduction of the response frequency. Therefore, the aim of the present investigation is to develop a generalised nonlinear FE model of the layered composite doubly curved shallow shell panel based on the HSDT mid-plane kinematics and Green-Lagrange nonlinear strain field. Subsequently, development of a customised computer code using the current higher-order nonlinear FE model including the direct iterative method and Newmark's time integration scheme. Further, the validity including the suppression of dynamic response frequency of the current higher-order nonlinear model has been established by comparing with the in-house experimental results. Finally, analysis has been extended to investigate the effect of different design parameters on the nonlinear time-dependent deflection responses of the smart laminated structure and the inferences provided in details.

Mathematical formulation

A generalized geometrically nonlinear mathematical model of the smart composite curved shell panel is developed. In this regard, the detailed FE electromechanical formulation is discussed in the following subsections.

Doubly curved shell element

Figure 1 shows the schematic diagram of a doubly curved shell panel of substrate thickness 'h' with piezoelectric layers of thickness 'h_p' constructed on a rectangular base of sides 'a' and 'b' considered for the present study. R_x and R_y are the principal radii of curvature of the shell panel along x and y-directions, respectively.

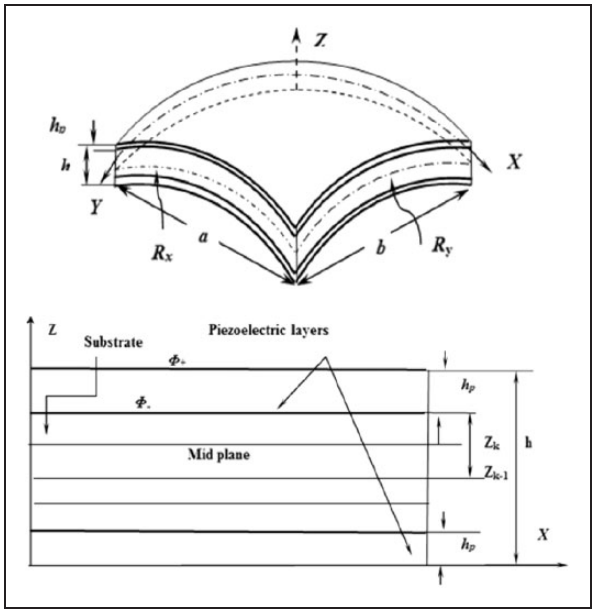

Figure 1. Geometry and dimension of the doubly-curved piezoelectric composite panel.

Kinematic model

In the present analysis, both the field variables within a shell element, i.e. the mechanical displacement (u, v, w) and the electric potential (ϕ^k) have been taken as the function of thickness-coordinate (z). In order to achieve generality, the displacement field along x and y-direction are considered to be third order polynomial and the variation of the displacement through the thickness is taken as the linear function of thickness coordinate at the mid-plane of shell element (i.e. $z=0$). The final form of the displacement field is conceded as in Singh and Panda[30]

$$\begin{aligned} u(x,y,z,t) &= u_0(x,y) + z\theta_x(x,y) + z^2\psi_x(x,y) \\ &\quad + z^3\lambda_x(x,y) \\ v(x,y,z,t) &= v_0(x,y) + z\theta_y(x,y) + z^2\psi_y(x,y) \\ &\quad + z^3\lambda_y(x,y) \\ w(x,y,z,t) &= w_0(x,y) + z\theta_z(x,y) \end{aligned} \tag{1}$$

Similarly, the electric potential variation within the panel is considered as the second order polynomial with three electrical degrees of freedom as in Benjeddou et al.[31]

$$\phi^k(x,y,z) = \phi_0^k(x,y) + z\phi_1^k(x,y) + z^2\phi_2^k(x,y) \tag{2}$$

where (u_0, v_0, w_0) denote the mid-plane displacements along x, y and z coordinates, respectively. θ_x and $\theta_y$are the shear rotations about the y and x-axes, respectively and other functions $(\psi_x, \psi_y, \lambda_x, \lambda_y)$are the higher-order terms defined in the mid-plane of the curved panel. 'θ_z' is the normal extension along z-axis also known as the 'thickness-stretching term'. The details of individual mechanical degrees of freedom functions at the mid-plane ($z=0$) can be seen in Singh et al.[32]

The three electrical degrees of freedom $(\phi_0^k, \phi_1^k, \phi_2^k)$ in any k^{th} piezoelectric layer are defined as follows

$$\phi_0^k = \frac{\phi_+^k + \phi_-^k}{2}, \quad \phi_1^k = \frac{\phi_-^k - \phi_+^k}{h_p}, \quad \phi_2^k = \frac{\phi_0^k + \phi_1^k}{2} \tag{3}$$

where $\phi_+^k$and ϕ_-^k are the electric potential at the top and bottom surfaces of a k^{th} piezoelectric layer and 'h_P' are the thickness of the piezoelectric layer. It is assumed that the inner electrode is grounded (i.e. $\phi_-^k = 0$) whereas the outer electrode is applied with an electric voltage (i.e. ϕ_+^k).

Strain–displacement relations

The general nonlinear strain–displacement relation for the laminated composite curved panel structure

with and without piezoelectric material is expressed by considering Green-Lagrange type nonlinearity[33]

$$\begin{Bmatrix}\varepsilon_{xx}\\ \varepsilon_{yy}\\ \varepsilon_{zz}\\ \varepsilon_{yz}\\ \varepsilon_{xz}\\ \varepsilon_{xy}\end{Bmatrix}=\begin{Bmatrix}\left(\frac{\partial u}{\partial x}+\frac{w}{R_x}\right)\\ \left(\frac{\partial v}{\partial y}+\frac{w}{R_y}\right)\\ \left(\frac{\partial w}{\partial z}\right)\\ \left(\frac{\partial v}{\partial z}+\frac{\partial w}{\partial y}-\frac{v}{R_y}\right)\\ \left(\frac{\partial u}{\partial z}+\frac{\partial w}{\partial x}-\frac{u}{R_x}\right)\\ \left(\frac{\partial u}{\partial y}+\frac{\partial v}{\partial x}+\frac{2w}{R_{xy}}\right)\end{Bmatrix}+\frac{1}{2}\begin{Bmatrix}\left[\left(\frac{\partial u}{\partial x}+\frac{w}{R_x}\right)^2+\left(\frac{\partial v}{\partial x}+\frac{w}{R_{xy}}\right)^2+\left(\frac{\partial w}{\partial x}-\frac{u}{R_x}\right)^2\right]\\ \left[\left(\frac{\partial u}{\partial y}+\frac{w}{R_{xy}}\right)^2+\left(\frac{\partial v}{\partial y}+\frac{w}{R_y}\right)^2+\left(\frac{\partial w}{\partial y}-\frac{v}{R_y}\right)^2\right]\\ \left[\left(\frac{\partial u}{\partial z}\right)^2+\left(\frac{\partial v}{\partial z}\right)^2+\left(\frac{\partial w}{\partial z}\right)^2\right]\\ 2\left[\frac{\partial u}{\partial z}\left(\frac{\partial u}{\partial y}+\frac{w}{R_{xy}}\right)+\frac{\partial v}{\partial z}\left(\frac{\partial v}{\partial y}+\frac{w}{R_y}\right)+\frac{\partial w}{\partial z}\left(\frac{\partial w}{\partial y}-\frac{v}{R_y}\right)\right]\\ 2\left[\frac{\partial u}{\partial z}\left(\frac{\partial u}{\partial x}+\frac{w}{R_x}\right)+\frac{\partial v}{\partial z}\left(\frac{\partial v}{\partial x}+\frac{w}{R_{xy}}\right)+\frac{\partial w}{\partial z}\left(\frac{\partial w}{\partial x}-\frac{u}{R_x}\right)\right]\\ 2\left[\left(\frac{\partial u}{\partial y}+\frac{w}{R_{xy}}\right)\left(\frac{\partial u}{\partial x}+\frac{w}{R_x}\right)+\left(\frac{\partial v}{\partial y}+\frac{w}{R_y}\right)\left(\frac{\partial v}{\partial x}+\frac{w}{R_{xy}}\right)+\left(\frac{\partial w}{\partial y}-\frac{v}{R_y}\right)\left(\frac{\partial w}{\partial x}-\frac{u}{R_x}\right)\right]\end{Bmatrix} \tag{4}$$

$$\{\varepsilon\}=\{\varepsilon_l\}+\{\varepsilon_{nl}\} \tag{5}$$

where $\{\varepsilon_l\}$and $\{\varepsilon_{nl}\}$ are the linear and the nonlinear strain tensors, respectively and the strain tensors are modified in matrix form as follows:

The expanded forms of the above linear/nonlinear strain terms are as below

$$\begin{Bmatrix}\varepsilon_x\\ \varepsilon_y\\ \varepsilon_z\\ \varepsilon_{yz}\\ \varepsilon_{xz}\\ \varepsilon_{xy}\end{Bmatrix}=\begin{Bmatrix}\varepsilon_x^0+zk_x^1+z^2k_x^2+z^3k_x^3\\ \varepsilon_y^0+zk_y^1+z^2k_y^2+z^3k_y^3\\ \varepsilon_z^0\\ \varepsilon_{yz}^0+zk_{yz}^1+z^2k_{yz}^2+z^3k_{yz}^3\\ \varepsilon_{xz}^0+zk_{xz}^1+z^2k_{xz}^2+z^3k_{xz}^3\\ \varepsilon_{xy}^0+zk_{xy}^1+z^2k_{xy}^2+z^3k_{xy}^3\end{Bmatrix}=[T_l]_{6\times21}\{\overline{\varepsilon_l}\}_{21\times1} \tag{6}$$

$$\begin{Bmatrix}\varepsilon_x^{nl}\\ \varepsilon_y^{nl}\\ \varepsilon_z^{nl}\\ \varepsilon_{yz}^{nl}\\ \varepsilon_{xz}^{nl}\\ \varepsilon_{xy}^{nl}\end{Bmatrix}=\begin{Bmatrix}\varepsilon_x^{nl_0}+zk_x^{nl_1}+z^2k_x^{nl_2}+z^3k_x^{nl_3}+z^4k_x^{nl_4}+z^5k_x^{nl_5}+z^6k_x^{nl_6}\\ \varepsilon_y^{nl_0}+zk_y^{nl_1}+z^2k_y^{nl_2}+z^3k_y^{nl_3}+z^4k_y^{nl_4}+z^5k_y^{nl_5}+z^6k_y^{nl_6}\\ \varepsilon_z^{nl_0}+zk_z^{nl_1}+z^2k_z^{nl_2}+z^3k_z^{nl_3}+z^4k_z^{nl_4}\\ \varepsilon_{yz}^{nl_0}+zk_{yz}^{nl_1}+z^2k_{yz}^{nl_2}+z^3k_{yz}^{nl_3}+z^4k_{yz}^{nl_4}+z^5k_{yz}^{nl_5}\\ \varepsilon_{xz}^{nl_0}+zk_{xz}^{nl_1}+z^2k_{xz}^{nl_2}+z^3k_{xz}^{nl_3}+z^4k_{xz}^{nl_4}+z^5k_{xz}^{nl_5}\\ \varepsilon_{xy}^{nl_0}+zk_{xy}^{nl_1}+z^2k_{xy}^{nl_2}+z^3k_{xy}^{nl_3}+z^4k_{xy}^{nl_4}+z^5k_{xy}^{nl_5}+z^6k_{xy}^{nl_6}\end{Bmatrix}=[T_{nl}]_{6\times38}\{\overline{\varepsilon_{nl}}\}_{38\times1} \tag{7}$$

The electric field 'E' can be expressed as the negative gradient of electric potential (ϕ)

$$\{E\}=\{E_x\,E_y\,E_z\}^T=\left\{-\partial\phi/\partial x\;\;-\partial\phi/\partial y\;\;-\partial\phi/\partial z\right\}^T \tag{8}$$

Now, substituting equation (2) in equation (8), the electric field variables along x, y and z-axes can be obtained as

$$\begin{aligned}\{E\}&=\{E_x\,E_y\,E_z\}^T=[T_\phi]_{3x8}\{E^0\}_{8x1}\\ \{E_i^0\}_{8x1}&=-\frac{\phi_e}{h_p}=[B_\phi]_{8x3}\{\phi_e\}_{3x1}\end{aligned} \tag{9}$$

The terms with superscripts '0', '1', '2–6' are the membrane, curvature and higher-order strain terms, respectively in their corresponding linear and nonlinear mid-plane strain matrices. The individual linear and the nonlinear strain terms are provided in Appendix 1. $[T_l]$, $[Tnl]$ and $[T_\phi]$ are the thickness coordinate matrices related to the linear, nonlinear strain–displacement relation and electric field potential relation, respectively and their details can be seen in Singh et al.[32]

Constitutive relations

The laminated composite shell panel is assumed to be consisting of a number of elastic substrate laminates integrated with piezoelectric actuating and sensing layers. The piezoelectric constitutive equations showing the coupling between the elastic and electric field are given by

$$\{D^E\}=[e]^T\{\varepsilon\}-[\in]\{E\} \tag{10}$$

$$\{\sigma\}=[Q]\{\varepsilon\}-[e]\{E\} \tag{11}$$

where $\{E\}$, $\{D^E\}$, $\{\sigma\}$ and $\{\varepsilon\}$ are the electric field, electric displacement, stress and strain vectors, respectively, whereas $[Q]$, $[e]$ and $[\in]$ are the constitutive matrix, piezoelectric stress matrix and dielectric constant matrix, respectively.

The piezoelectric stress matrices for PZT/polyvinylidene difluoride (PVDF) and active fiber composite (AFC)/macro fiber composite (MFC) are given as

$$\left[e^k\right]_{PVDF/PZT} = \begin{bmatrix} 0 & 0 & 0 & e_{14} & e_{15} & 0 \\ 0 & 0 & 0 & e_{24} & e_{25} & 0 \\ e_{31} & e_{32} & e_{33} & 0 & 0 & e_{36} \end{bmatrix},$$
$$\left[e^k\right]_{AFC/MFC} = \begin{bmatrix} e_{11} & e_{12} & 0 & 0 & 0 & e_{16} \\ 0 & 0 & 0 & e_{24} & e_{25} & 0 \\ 0 & 0 & 0 & e_{34} & e_{35} & 0 \end{bmatrix}^k \tag{12}$$

The dielectric constant matrix is given as

$$\left[\in^k\right] = \begin{bmatrix} \in_{11} & \in_{12} & 0 \\ \in_{12} & \in_{22} & 0 \\ 0 & 0 & \in_{33} \end{bmatrix}^k \tag{13}$$

Energy equation

The structural displacements due to external electromechanical loading and the total potential energy of the system are expressed as

$$T_p = \frac{1}{2}\left[\sum_{i=1}^{n}\int_v \left\{\varepsilon^k\right\}^T\left\{\sigma^k\right\}\mathrm{d}v - \int_v \{E_i\}^T\left\{D_s^E\right\}\mathrm{d}v - \int_v \{E_i\}^T\left\{D_a^E\right\}\mathrm{d}v\right] \tag{14}$$

where the subscript 'i' represents 'a' and 's' for the actuator and sensor, respectively. Substituting the equations (12) and (13) the above equation can be rewritten as

$$T_P = {}^1/_2\int_A \begin{pmatrix} \{\overline{\varepsilon_l}\}^T[D_1]\{\overline{\varepsilon}\} + \{\overline{\varepsilon}\}^T[D_2]\{\overline{\varepsilon_{nl}}\} \\ +\{\overline{\varepsilon_{nl}}\}^T[D_3]\{\overline{\varepsilon}\} + \{\overline{\varepsilon_{nl}}\}^T[D_4]\{\overline{\varepsilon_{nl}}\} \\ -\{\overline{\varepsilon}\}^T[D_5]\left\{E^0\right\} - \left\{E^0\right\}^T[D_6]\{\overline{\varepsilon}\} - \{\overline{\varepsilon_{nl}}\}^T[D_7]\left\{E^0\right\} \\ -\left\{E^0\right\}^T[D_8]\{\overline{\varepsilon_{nl}}\} - \left\{E^0\right\}^T[D_9]\left\{E^0\right\} \end{pmatrix}\mathrm{d}A \tag{15}$$

where $[D_1]$, $[D_2]$, $[D_3]$, $[D_4]$, $[D_5]$, $[D_6]$, $[D_7]$, $[D_8]$ and $[D_9]$ are the linear and nonlinear, uncoupled and coupled electromechanical material stiffness matrices.

System governing equation

The governing equation of motion of the structural system under the dynamic load is obtained by using the classical Hamilton's principle. This is also known as the dynamic version of the principle of minimum potential energy (PMPE) and can be expressed in terms of Lagrangian 'L' as

$$I = \int_{t1}^{t2} L\mathrm{d}t = \int_{t1}^{t2} (T_P - T_{KE})\mathrm{d}t \tag{16}$$

where the kinetic energy (T_{KE}) of the laminate is given by

$$T_{KE} = \frac{1}{2}\sum_{k=1}^{n}\int_v \left\{\dot{d}\right\}^T\rho^k\left\{\dot{d}\right\}\mathrm{d}v \tag{17}$$

where ρ^k is the mass density of k^{th} layer. From the above minimum potential energy and Hamilton's principle

$$\delta\int_{t1}^{t2} (T_P - T_{KE})\mathrm{d}t = 0 \tag{18}$$

In the present study, a nine noded Lagrangian isoparametric quadrilateral element is employed to discretize the laminated composite panel domain. The element geometry, displacement and electric potential vectors over each element using isoparametric concept are written in terms of interpolation function and expressed as

$$x = \sum_{i=1}^{9} N_i x_i,\ y = \sum_{i=1}^{9} N_i y_i,\ \{d_0\} = \sum_{i=1}^{9} N_i\{d_0 i\};$$
$$\{\phi_{e0}\} = \sum_{i=1}^{9} N_i\{\phi_{e0} i\} \tag{19}$$

Here, $[N_i]$ is the interpolation function of the ith node, x_i and y_i are the geometry coordinates in x and y-direction, respectively. $\{d_{0i}\} = [u_{0i},\ v_{0i},\ w_{0i}, \theta_{xi}, \theta_{yi}, \theta_{zi}, \psi_{xi}, \psi_{yi}, \lambda_{xi}, \lambda_{yi}]$ and $\{\phi_{e0i}\} = \left\{\phi_{0i}\quad \phi_{1i}\quad \phi_{2i}\right\}$ are the unknown mechanical displacement and the electric potential vector for the i^{th} node of the element.

Similarly, the mid-plane linear and nonlinear strain vectors in terms of their nodal displacement vector can be written as

$$\{\overline{\varepsilon_l}\}_{21\times1} = [B_l]_{21\times10}\{d_o\}_{10\times1},\ \{\overline{\varepsilon_{nl}}\}_{38\times1} = \frac{1}{2}[A]_{38\times27}[G]_{27\times1}\{d_0\}_{10\times1},$$
$$\left\{E_i^0\right\}_{8x1} = -\frac{\phi_e}{h_p} = \left[B_\phi\right]_{8x3}\{\phi_e\}_{3x1},\ \left[B_\phi\right] = -\left[\frac{N_j}{h_p}\right]$$
$$(\mathrm{j} = 1,\ 2\ldots,9) \tag{20}$$

where corresponding to $i = 3$, the layer is considered to be PVDF/PZT, similarly, 1 refers to the AFC layer, h_{p} is the thickness of the PVDF sensor layer and

spacing between the electrodes of interdigitated electrodes (IDE) for AFC layer. Further, $[B_l]$, $[B_{nl}]$ and $[B_\phi]$ are the linear, nonlinear strain–displacement matrices and electric field-electric potential matrices, respectively. These matrices along with $[G]$ matrix can be obtained by multiplying corresponding differential operator matrix and interpolation matrix. [A] is the function of displacements corresponding to the nonlinear strain. The individual terms of matrices [A], $[B_l]$, $[B_{nl}]$, $[B_\phi]$ and [G] are provided in Singh et al.[32]

Substituting equations (15) and (17) in equation (18) and using equation (20) the system governing equation can be conceded as

$$[M]\left\{\ddot{d}\right\} + \left[\overline{K}(\{d\})\right]\{d\} = \{F_m\} + \{F_e\} \tag{21}$$

$$\begin{aligned}\left[\overline{K}(\{d\})\right] = [K_d + K_{dnl}] - [K_{di} + K_{dnli}]\left[K_{\phi\phi}\right]^{-1} \\ \times \left[K_{id} + \frac{1}{2}K_{idnl}\right]\end{aligned} \tag{22}$$

$$\{F_m\} = \int_{-1}^{1}\int_{-1}^{1} [N]^T\{q\}|J|\mathrm{d}\xi\mathrm{d}\eta \tag{23}$$

$$\begin{aligned}\{F_e\} &= \int_{-1}^{1}\int_{-1}^{1} [N]^T\sigma_E(x,y)|J|\mathrm{d}\xi\mathrm{d}\eta \\ &= \frac{\in_{33}}{(z_{k-1}-z_k)}\int_{-1}^{1}\int_{-1}^{1} [N]^T\{\phi_e\}|J|\mathrm{d}\xi\mathrm{d}\eta\end{aligned} \tag{24}$$

$$\begin{aligned}[M] &= \int_{-1}^{1}\int_{-1}^{1} [N]^T[\overline{m}][N]|J|\mathrm{d}\xi\mathrm{d}\eta; \\ [\overline{m}] &= \sum_{k=1}^{n}\int_{z_k}^{z_{k+1}} [f_{mz}]^T\left[\rho^k\right][f_{mz}]\end{aligned} \tag{25}$$

$$[K_d] = \int_{-1}^{1}\int_{-1}^{1} [B_l]^T[D_1][B_l]|J|\mathrm{d}\xi\mathrm{d}\eta \tag{26}$$

$$\begin{aligned}[K_{dnl}] = \frac{1}{2}\int_{-1}^{1}\int_{-1}^{1} [B_l]^T[D_2][B_{nl}]|J|\mathrm{d}\xi\mathrm{d}\eta \\ + \int_{-1}^{1}\int_{-1}^{1} [B_{nl}]^T[D_3][B_l]|J|\mathrm{d}\xi\mathrm{d}\eta \\ + \frac{1}{2}\int_{-1}^{1}\int_{-1}^{1} [B_{nl}]^T[D_4][B_{nl}]|J|\mathrm{d}\xi\mathrm{d}\eta\end{aligned} \tag{27}$$

$$[K_{di}] = \int_{-1}^{1}\int_{-1}^{1} [B_l]^T[D_5]\left[B_{\phi i}\right]|J|\mathrm{d}\xi\mathrm{d}\eta,\ [K_{di}] = [K_{id}]^T \tag{28}$$

$$\begin{aligned}[K_{dnli}] &= \int_{-1}^{1}\int_{-1}^{1} [B_{nl}]^T[D_7]\left[B_{\phi i}\right]|J|\mathrm{d}\xi\mathrm{d}\eta; \\ [K_{idnl}] &= [K_{dnli}]^T\end{aligned} \tag{29}$$

$$\left[K_{\phi\phi i}\right] = \int_{-1}^{1}\int_{-1}^{1} \left[B_{\phi i}\right]^T[D_9]\left[B_{\phi i}\right]|J|\mathrm{d}\xi\mathrm{d}\eta \tag{30}$$

Here, $i = a$ and s stand for the actuator and sensor, respectively.

In the above equations, $[M]$ is the mass matrix, $[K_d]$ and $[K_{dnl}]$ are the linear and nonlinear elastic stiffness matrices, respectively. $[K_{id}]$ and $[K_{idnl}]$ $(i = a, s)$ are the linear and nonlinear electro-elastic coupling stiffness matrices for the sensor and actuator while, $[K_{di}]$ and $[K_{dnli}]$ $(i = a, s)$ are the linear and nonlinear elastic-electro coupling matrices for the sensor and actuator, respectively. $\{F_m\}$ is the applied mechanical load and $\{F_e\}$ is the applied electric force vector whereas, $\sigma_E(x, y)$ is the surface charge density.

Solution technique

The desired nonlinear responses have been obtained by solving the corresponding governing equilibrium equations using the direct iterative method in conjunction with the nonlinear FEM. The governing equilibrium equation for the transient system can be rewritten as

$$\left[\hat{K}\left(\left\{d_{n+1}\right\}\right)\right]\left\{d_{n+1}\right\} = \left\{\hat{F}\right\}_{n,n+1} \tag{31}$$

The subscript $n+1$ refers to the time t_{n+1} at which the solution is required

$$\left[\hat{K}\left(\left\{d_{n+1}\right\}\right)\right] = \left[K\left(\left\{d_{n+1}\right\}\right)\right] + a_0[M]_{n+1} \tag{32}$$

$$\left\{\hat{F}\right\}_{n,n+1} = \{F\}_{n+1} + [M]_{n+1}\left\{\hat{A}\right\}_s \tag{33}$$

$$\begin{aligned}\left\{\hat{A}\right\}_n &= a_0\{d\}_n + a_2\left\{\dot{d}\right\}_n + a_3\left\{\dot{d}\right\}_n,\ \left\{\hat{B}\right\}_n \\ &= a_1\{d\}_n + a_4\left\{\dot{d}\right\}_n + a_5\left\{\dot{d}\right\}_n\end{aligned} \tag{34}$$

where a_i, $i = 1, 2, \ldots 8$ are defined as

$$\begin{aligned}&\overline{\alpha} = 0.25, \quad \overline{\beta} = 0.5, \quad a_0 = \frac{1}{\overline{\alpha}\delta t^2}, \quad a_1 = \frac{\overline{\beta}}{\overline{\alpha}\delta t}, \quad a_2 = \frac{1}{\overline{\alpha}\delta t} \\ &a_3 = \frac{1}{2\overline{\alpha}} - 1, \quad a_4 = \frac{\overline{\beta}}{\overline{\alpha}} - 1, \quad a_5 = 0.5\delta t\left(\frac{\overline{\beta}}{\overline{\alpha}} - 2\right), \\ &a_6 = \delta t\left(1 - \overline{\beta}\right), \quad a_7 = \delta t\,\overline{\beta}\end{aligned} \tag{35}$$

The nonlinear time-dependent governing equation, i.e. equation (31) has been solved by an iterative method. For every time step, the direct iterations are applied to obtain the equilibrium and the stiffness and force vectors are updated accordingly. The details of the transient solution steps can be seen in Saviz.[29]

Nonlinear finite element

The algorithm for applying nonlinear finite element (NFEM) in finding the solution of the governing

nonlinear equilibrium equation (equation (21)) is presented in the form of a flowchart in Figure 2.[34]

Direct iterative method

The direct iterative method is incorporated along with NFEM to find the nonlinear solution at the rth iteration knowing the elemental stiffness at the $(r-1)$th iteration using following assembled set of equations.

$$\left[\overline{K}\left(\{d_0\}^{r-1}\right)\right]\{d_0\}^{r} = \{F\} \tag{36}$$

where $\overline{K}\left(\{d_0\}^{r-1}\right)$is the global known nonlinear stiffness and $\{d_0\}^{r}$is the unknown solution at the rth iteration.

Boundary constraints

In order to avoid the rigid body motion for the numerical analysis, various support conditions (clamped, C; simply supported, S; hinged, H; and free, F) have been imposed on the edges of the curved shell panels. The details of the restricted degrees of freedoms for different support conditions are presented in Table 1.

Results and discussion

The geometrically nonlinear transient bending responses of curved piezoelectric composite shell panels are presented using the presently developed higher-order mathematical model. The developed mathematical model is incorporated into a computer programme written in MATLAB R2012b environment to get the desired linear and nonlinear transient solutions. For the computation of the responses and to avoid the locking a selective reduced integration, i.e. (3×3) and (2×2) points are considered for the bending and the shear stress cases. In addition, the material properties and the details of support conditions are given in Tables 1 and 2, respectively. The NFEM equation is linearized using the direct

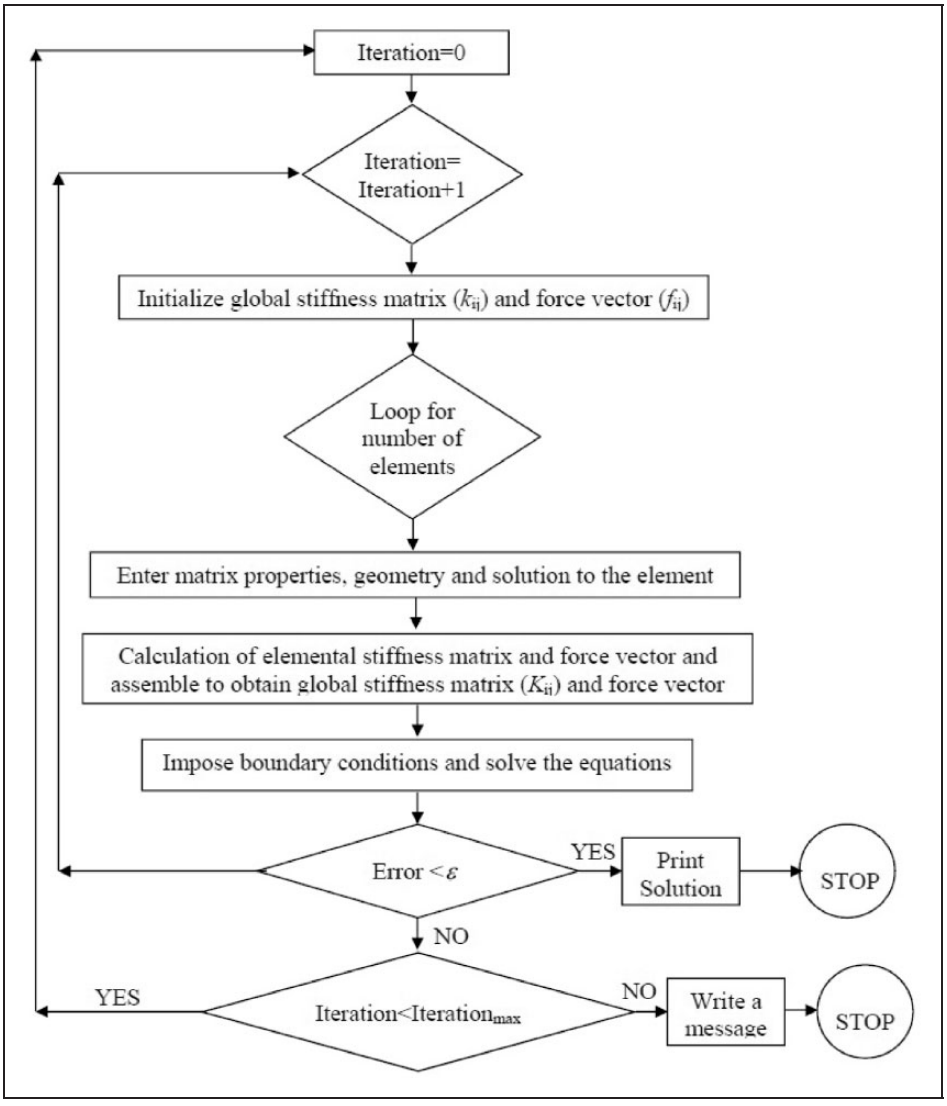

Figure 2. Nonlinear finite element programme for the solution of the model.

Table 1. Material properties of substrate and piezoelectric layers.

Properties	Substrate[12]	MFC[12]	PVDF[35]	Estimated properties	AFC[15]
E_1 (GPa)	150.0	30.25	2.0	C_{11} (GPa)	32.6
E_2 (GPa)	9.0	15.99	2.0	C_{22} (GPa)	7.2
ν_{12}	0.25	0.306	0.29	C_{12} (GPa)	4.3
G_{12} (GPa)	7.1	5.52	0.775	C_{66} (GPa)	1.05
G_{13} (GPa)	7.1	11.82	0.775	C_{44} (GPa)	1.29
G_{23} (GPa)	2.5	4.54	0.400	C_{55} (GPa)	1.29
e_{31} ($cm-^2$)	–	–	0.046	e_{11}(cm^{-2})	−6.76
e_{32} (cm^{-2})	–	–	0.046	e_{12}(cm^{-2})	−0.076
d_{11} (pC/N)	–	385.56	–	–	–
d_{12} (pC/N)	–	−171.43	–	–	–
ϵ_{33} (nFm^{-1})	–	–	0.1062		
ϵ_{11} (nFm^{-1})	–	14.3	–	ϵ_{11} (nFm^{-1})	8.599
ρ (Kgm^{-3})	1600	5019	1800	ρ (Kgm^{-3})	6700

MFC: macro fiber composite; PVDF: polyvinylidene difluoride; AFC: active fiber composite.

Table 2. Details of support conditions.

Type	Locations	Restricted degrees of freedom
CCCC	At $x=0$, a and $y=0$, b	$u_0 = v_0 = w_0 = \theta_x = \theta_z = \psi_x = \psi_y = \lambda_x = \lambda_y = 0$
SSSS	At $x=0$, a	$v_0 = w_0 = \theta_y = \theta_z = \psi_y = \lambda_y = 0$
	At $y=0$, b	$u_0 = w_0 = \theta_x = \theta_z = \psi_x = \lambda_x = 0$
SCSC	At $x=0$, a	$v_0 = w_0 = \theta_y = \theta_z = \psi_y = \lambda_y = 0$
	At $y=0$, b	$u_0 = v_0 = w_0 = \theta_x = \theta_y = \theta_z = \psi_x = \psi_y = \lambda_x = \lambda_y = 0$
HHHH	At $x=0$, a	$u_0 = v_0 = w_0 = \theta_y = \theta_z = \psi_x = \psi_y = \lambda_x = \lambda_y = 0$
	At $y=0$, b	$u_0 = v_0 = w_0 = \theta_x = \theta_z = \psi_x = \psi_y = \lambda_x = \lambda_y = 0$
	At $y=0$, b	$u_0 \neq v_0 \neq w_0 \neq \theta_x \neq \theta_y \neq \theta_z \neq \psi_x \neq \psi_y \neq \lambda_x \neq \lambda_y$

iterative method and Newmark's time integration algorithm (constant-average-acceleration method) with a time step of 50×10^{-5} s. Two types of the sensor and actuator arrangements namely collocated (sensor is placed adjacent to the actuator) and non-collocated (sensor is placed away from the actuator), shown in Figure 3 are considered in the present analysis. The collocated and non-collocated configurations are denoted by a notation 'C' and 'NC' respectively throughout the analysis. An anti-symmetric cross-ply square ($a/b=1$) smart plate with the collocated configuration (C-0/90/0/90/AFC/PVDF) subjected to uniformly distributed load (UDL) ($q_0 = 1 \times 10^3$ N/m^2) under simply supported boundary condition is considered throughout the present study unless specified otherwise. The efficacy and accuracy of present developed nonlinear coupled FE model are checked through the convergence of the linear and nonlinear transient bending responses followed by the validation study. A wide variety of numerical examples are solved to bring out the effect of different geometrical parameters (aspect ratio, thickness ratio, curvature ratio), support conditions and shell forms) and arrangement of sensor/actuator configuration on the linear/nonlinear transient bending responses are discussed in detail in the following sections. The non-dimensional formula for transient displacement is considered as follows

Linear/nonlinear central displacement $\left(\overline{w}_{L/NL}\right) = \frac{W_{L/NL}}{h}$where subscript '$L$' and '$NL$' denote the linear and nonlinear responses respectively.

Convergence and comparison study

In order to establish the stability and efficacy of the presently developed coupled nonlinear FE model to compute the linear and nonlinear transient bending responses, the convergence test and validation study have been carried out and presented in this section. It is seen in Figure 4 that the linear transient responses computed for two-layer thin ($a/h=100$) angle-ply ($45^\circ/-45^\circ$) laminated composite plate are converging well with mesh refinement. Based on the convergence study (6×6) mesh has been employed for throughout the present study. So as to validate the linear transient responses a four-layer antisymmetric

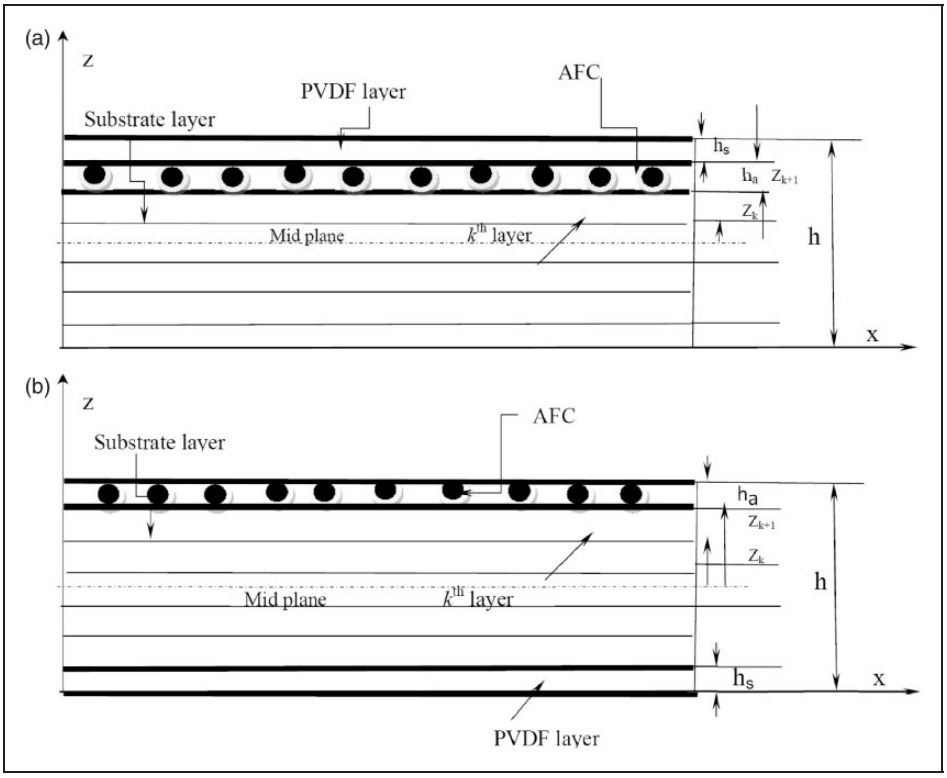

Figure 3. Different arrangements of sensing and actuating layers (Collocated-C and non-collocated-NC).

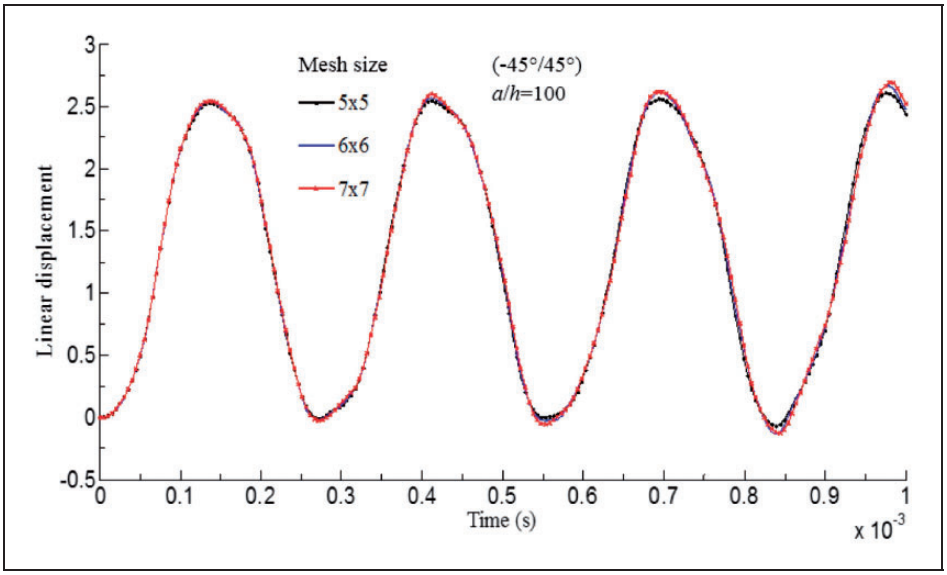

Figure 4. Convergence of linear transient response of two-layer thin (a/h = 100) angle-ply (−45°/45°) laminated composite plate.

angle-ply (45°/−45°/45°/−45°) laminated composite plate example as in Chen et al.[36] is considered. The results computed using the present model is plotted in Figure 5 which shows good agreement with that of the published results.

Subsequently, to validate the nonlinear transient bending responses, simply supported single/doubly curved panel examples[37,38] are considered. The geometrical parameters and material properties are taken to be similar to the considered references. The present results along with the reference values are presented in Figures 6 and 7 for the cylindrical and spherical composite shell panel, respectively. It is seen that the present transient responses are slightly higher when compared to that of the reference values. It is mainly due to the type of displacement field model (highly flexible) and the solution technique adopted in the present case in comparison to that adopted in the reference model. It is worthy to mention that the present model is based on the HSDT mid-plane

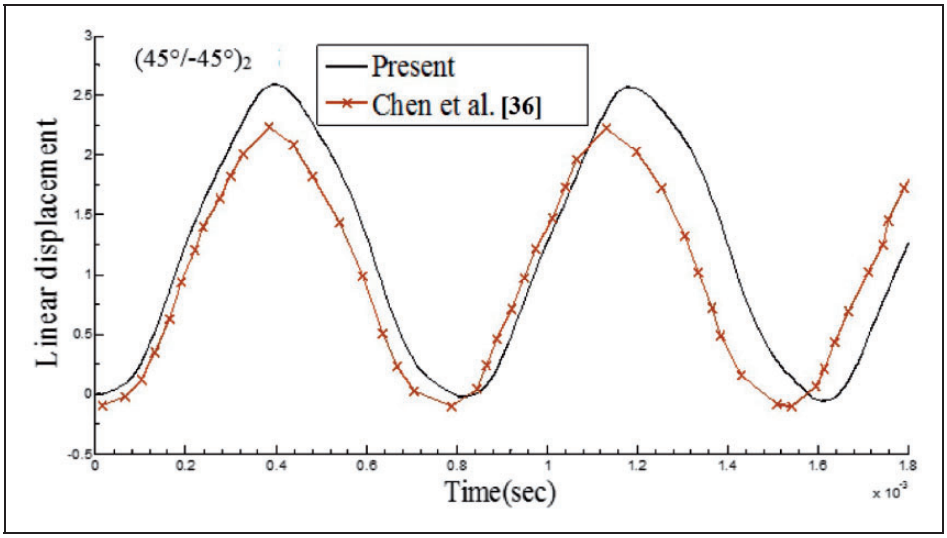

Figure 5. Comparison study of linear transient response of antisymmetric four-layer angle-ply (45°/−45°/45°/−45°) laminated composite plate.

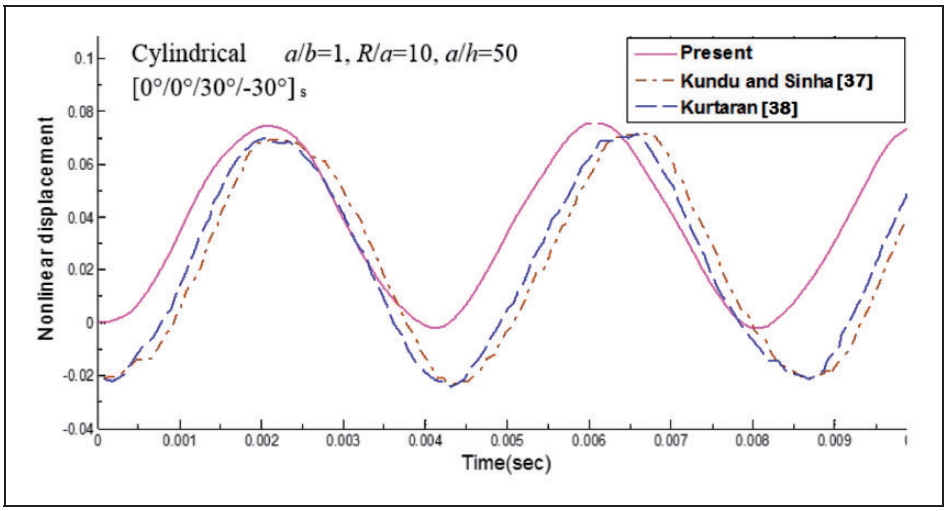

Figure 6. Validation study of nonlinear transient response of simply supported composite cylindrical shell panel.

kinematics and full geometrical nonlinearity in Green-Lagrange sense. In addition, the present model also includes all the nonlinear higher-order strain terms arising during formulation. Further, the present solutions are obtained using a direct iterative method in association with the FEM steps. However, both the references[37,38] have adopted the FSDT kinematics and von-Karman nonlinear strain and solved via Newton–Raphson technique in association with the generalized differential quadrature method in Kundu and Sinha[37] and Kurtaran[38], respectively.

Experimental study

The active suppression of dynamic responses has been examined and presented in this section. The experimental setup utilised for this purpose is shown in Figure 8. A carbon/epoxy composite plate model (1) is taken as a host structure and bonded with PZT/sp-5H patches (2) on its top and bottom faces. Two PZT-5H (5.0 cm × 1.0 cm × 0.1 cm) patches are surface bonded symmetrically at the top and bottom faces of the cantilever composite plate (10 cm × 10 cm × 0.15 cm) at a distance of 1.0 cm from each side of the plate surface using a commercial glue Araldite. A sinusoidal excitation force (1.5 N) at certain frequency (30 Hz) is given by the exciter (3) to the substrate using an amplifier (4). An accelerometer (5) is mounted on the tip of the PZT bonded composite plate to sense the physical signal, i.e. acceleration response and the corresponding electric analogue signal is fed to the data acquisition cDAQ/9178 (6) for the transformation into the corresponding digital signal. The acceleration obtained is integrated using the presently developed LabVIEW graphical programe to get the deflection response on the display window (7). The dynamic responses of the substrate

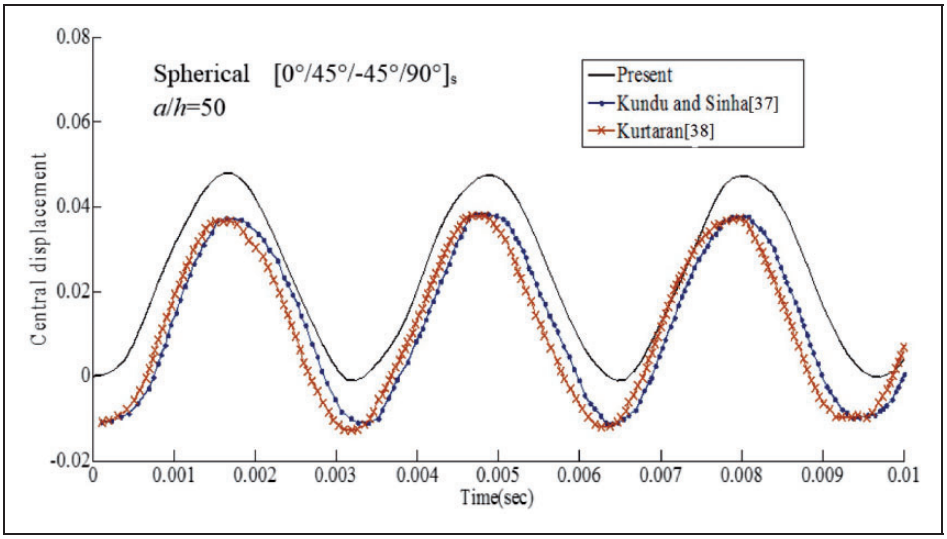

Figure 7. Validation study of nonlinear transient response of simply supported composite spherical shell panel.

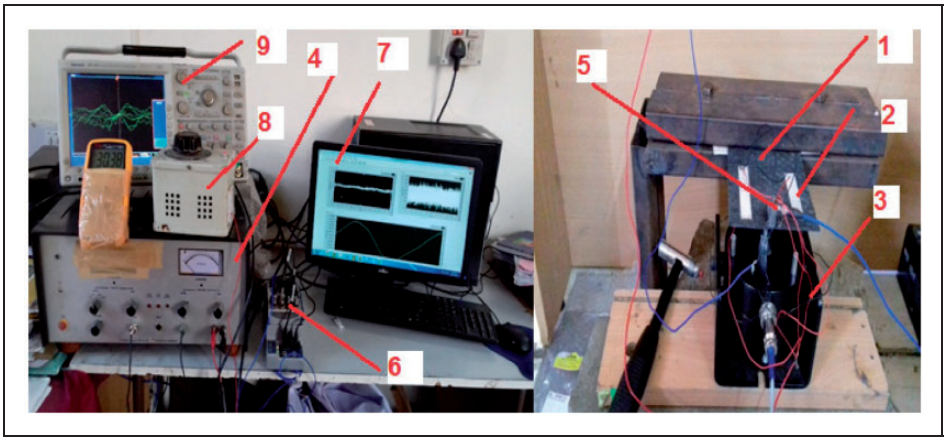

Figure 8. Experimental set up for transient analysis.

bonded with PZT patches, applied with different electric voltages such as 10 V and 20 V using an auto-transformer (8) are obtained. These experimentally obtained values are compared with the corresponding numerical solutions computed using the present geometrically nonlinear higher order FE model and presented in Figure 9. The importance of using the higher-order mid-plane kinematics in conjunction with the Green-Lagrange geometrical nonlinearity for modeling the smart laminated composite structures is clearly evident from the results. Moreover, the suppression of the dynamic responses with the increase in electric voltage applied can be seen from the results.

Numerical illustrations

The presently developed nonlinear higher-order model is employed by varying different geometrical parameter including the shell configuration for the prediction of the nonlinear transient responses of the laminated smart composite shell panel structure. For the computation of the desired responses a

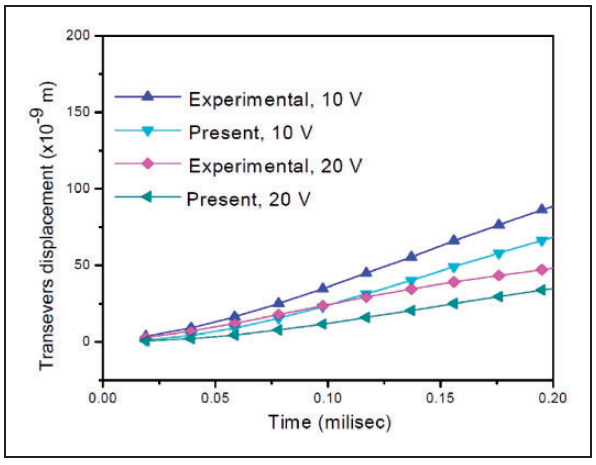

Figure 9. Comparison of dynamic responses of carbon/epoxy plate bonded with PZT patches.

composite shell panel with a substrate layer of thickness 0.002 m surface bonded or embedded with the MFC/AFC actuator with the electrode spacing 0.5 mm, poled in fiber direction and PVDF sensor

poled in thickness direction has been considered. Both the sensor and actuator are considered to have equal thickness of 0.0005 m. The dynamic bending responses are computed using presently developed nonlinear FE computer code in MATLAB environment. The influence of different geometrical parameters such as the aspect ratios (a/b), the thickness ratios (b/h), the support conditions and different sensor/actuator configuration (non-collocated and collocated) is investigated in this present study.

Effect of curvature ratio (R/b) on nonlinear transient bending responses of single/doubly curved piezoelectric composite shell panels

As the composite shell panels use flexural strength as well as the membrane actions about the mid-surface, it becomes very essential to examine the effect of curvature ratio on the transient responses with large amplitude. In this regard the nonlinear transient bending responses of two different forms of piezoelectric composite shell panels (i.e. cylindrical and hyperboloid) are computed at three different values of curvature ratios ($R/b = 5$, 10 and 100) for collocated (C-0/90/90/0/AFC/PVDF) and non-collocated (NC-AFC /0/90/90/0/PVDF) sensor/actuator arrangements. It is clearly evident from the results presented in Figures 10 and 11 that the non-collocated arrangement is showing

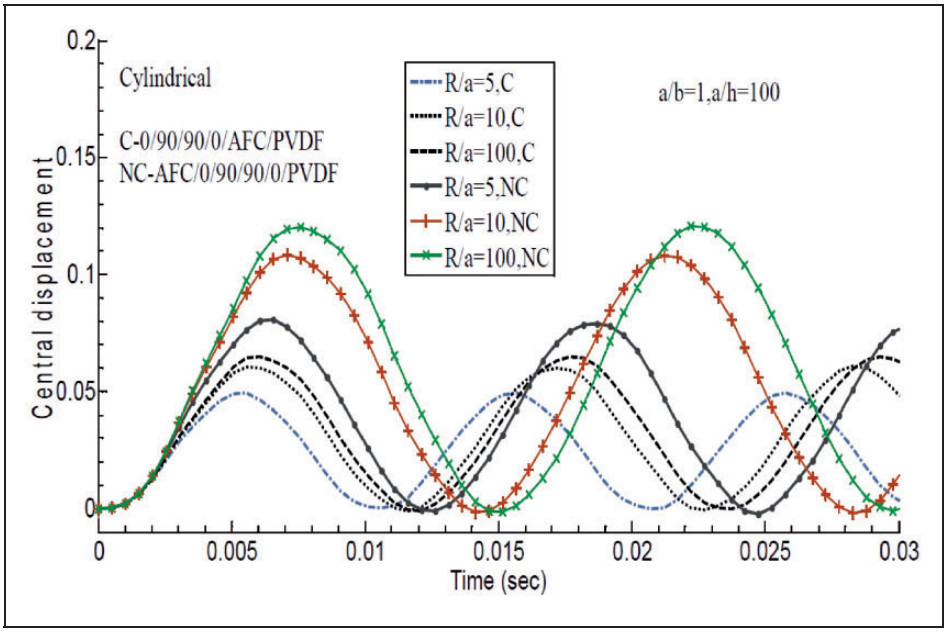

Figure 10. Effect of curvature ratio on nonlinear transient response of simply supported composite cylindrical shell panel.

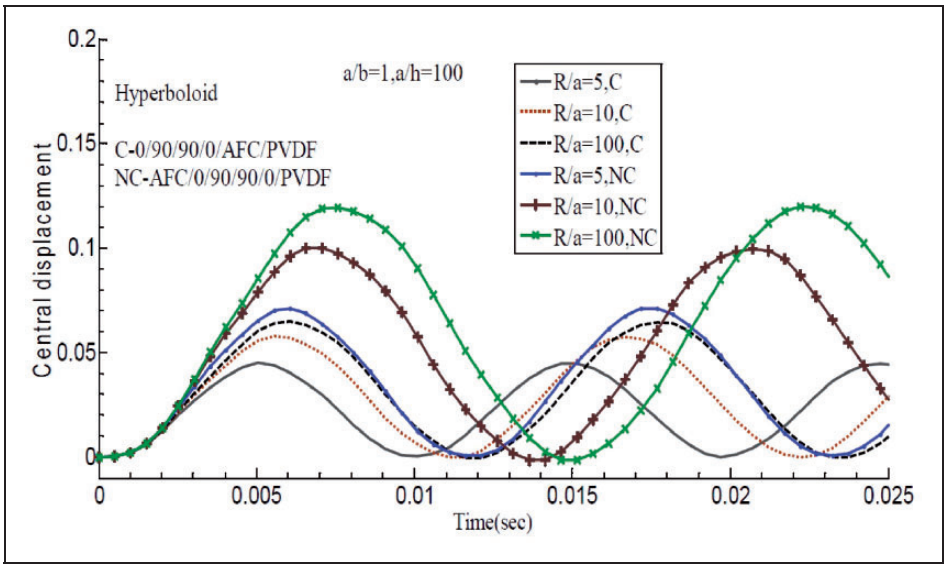

Figure 11. Effect of curvature ratio on nonlinear transient response of simply supported composite hyperboloid shell panel.

higher values of dynamic responses irrespective of shell geometry. It is also noted that the increase in curvature ratio improves the flexibility of the structural shell panels and thus intensifies the large amplitude deformation.

Effect of aspect ratio (a/b) on nonlinear transient bending responses of single/doubly curved piezoelectric composite shell panels. The aspect ratio (a/b) defines the shape of the structural component, i.e. square or rectangular geometry and it affects the strength of the structural component directly because of the variation of the moment of inertia. The nonlinear transient bending responses of two different forms of piezoelectric composite curved (cylindrical and ellipsoid) panels are computed for three different values of aspect ratios ($a/b = 0.5$, 1.0 and 1.5) with collocated (C-0/90/90/0/AFC/PVDF) and non-collocated (NC-AFC/0/90/90/0/PVDF) sensor/actuator arrangements. It is clear from Figures 12 and 13 that the cylindrical shell panels undergo the highest value of large amplitude dynamic displacement whereas the ellipsoid panels exhibit the smallest one for the same value of UDL mechanical loading. Moreover, the increase in aspect ratio reduces the dynamic responses to a great extent in all the cases.

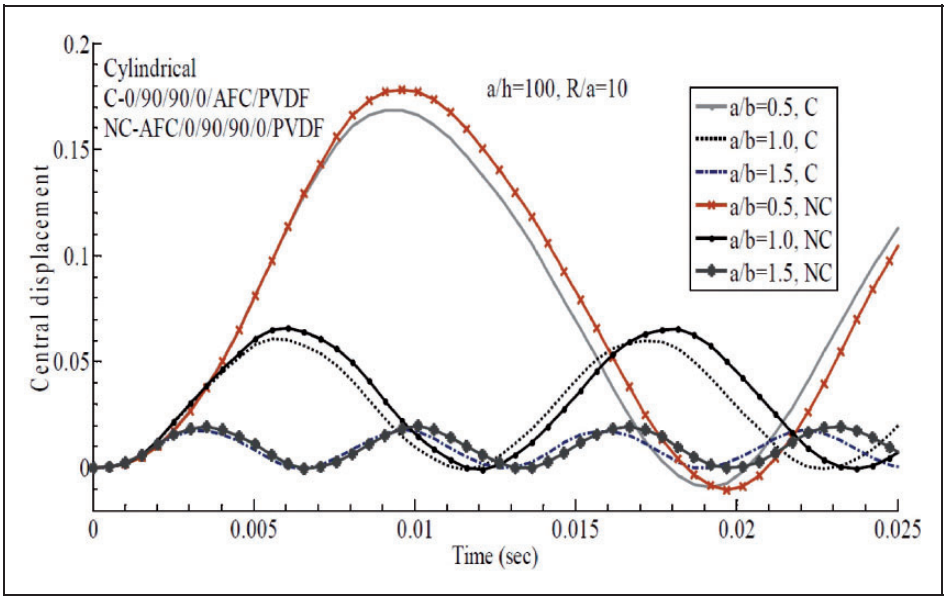

Figure 12. Effect of aspect ratio on nonlinear transient response of simply supported composite cylindrical shell panel.

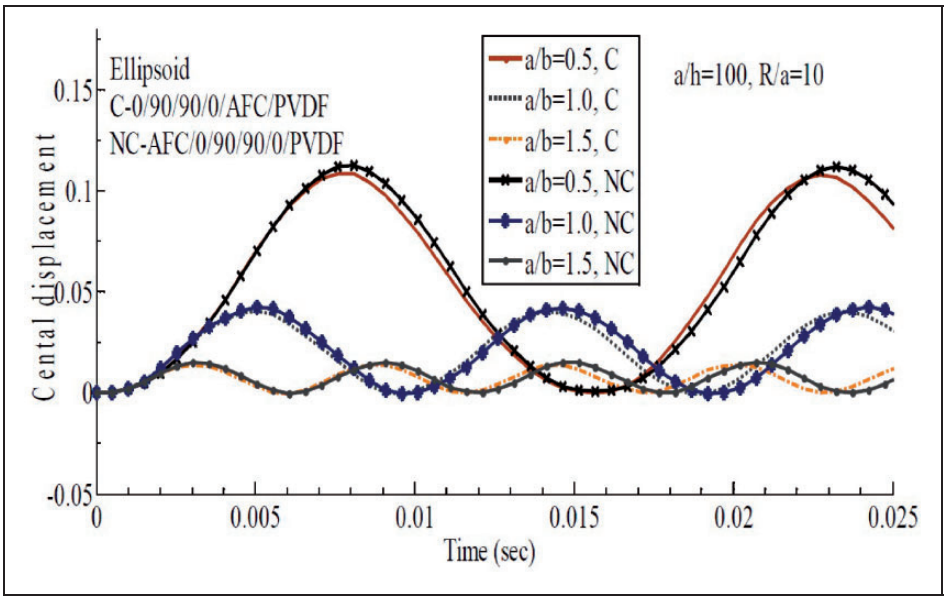

Figure 13. Effect of aspect ratio on nonlinear transient response of simply supported composite ellipsoid shell panel.

Effect of thickness ratio (a/h) on nonlinear transient bending responses of single/doubly curved piezoelectric composite shell panels. The thickness ratio of the structure and/or structural component governs the type of shear deformation theory used for analyzing the behaviour of laminated composite plate/shell structures. The effect of thickness ratio ($a/h = 50$, 80, 100) on the nonlinear transient bending responses of cylindrical and hyperboloid shell panels with two types sensor/actuator arrangements (i.e. C-0/90/0/90/AFC/PVDF and NC-AFC/0/90/0/90/PVDF) is investigated in this section. It is noted from the results presented in Figures 14 and 15 that the nonlinear dynamic deformation is more in case of the hyperboloid shell panel in comparison to the ellipsoid shell. It is also clear that the NC has larger dynamic responses as compared to C and the magnitude of the response increases monotonically with the thickness ratio irrespective of shell forms. It is also interesting to note that the effect of sensor/actuator arrangement is less significant in case of cylindrical shell whereas it is more in case of hyperboloid shells.

Effect of support conditions on nonlinear transient bending responses of single/doubly curved piezoelectric composite shell panels. The type of support conditions imposed to any plate/shell structural component affects its' stiffness/flexibility and therefore it becomes essential to analyze its' influence on the structural responses. In this section, the nonlinear dynamic bending responses smart composite curved panel with NC

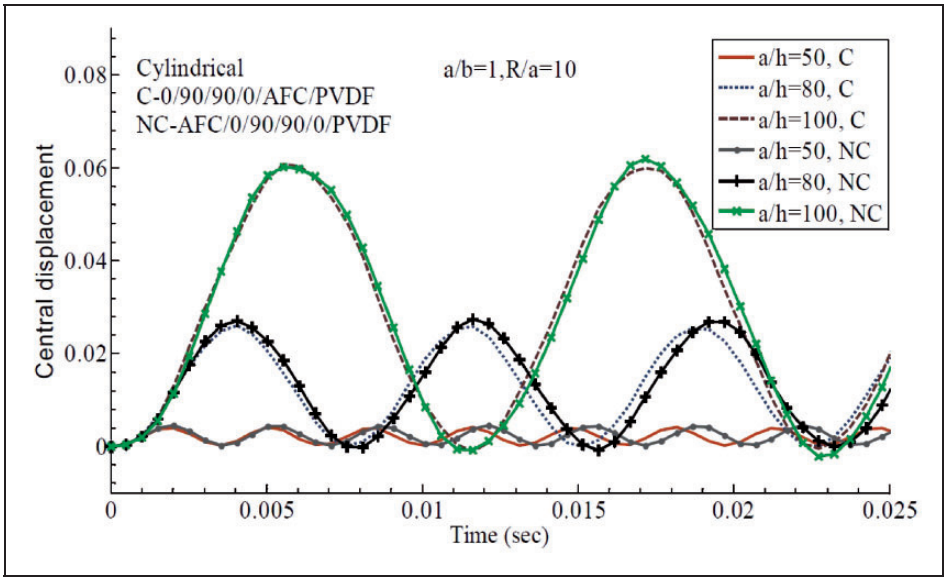

Figure 14. Effect of thickness ratio on nonlinear transient response of simply supported composite cylindrical shell panel.

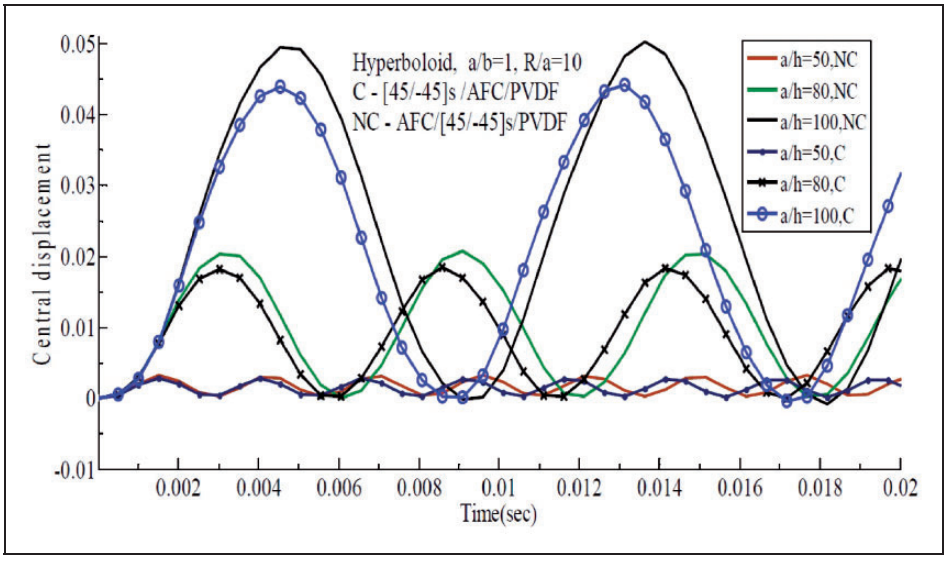

Figure 15. Effect of thickness ratio on nonlinear transient response of simply supported composite hyperboloid shell panel.

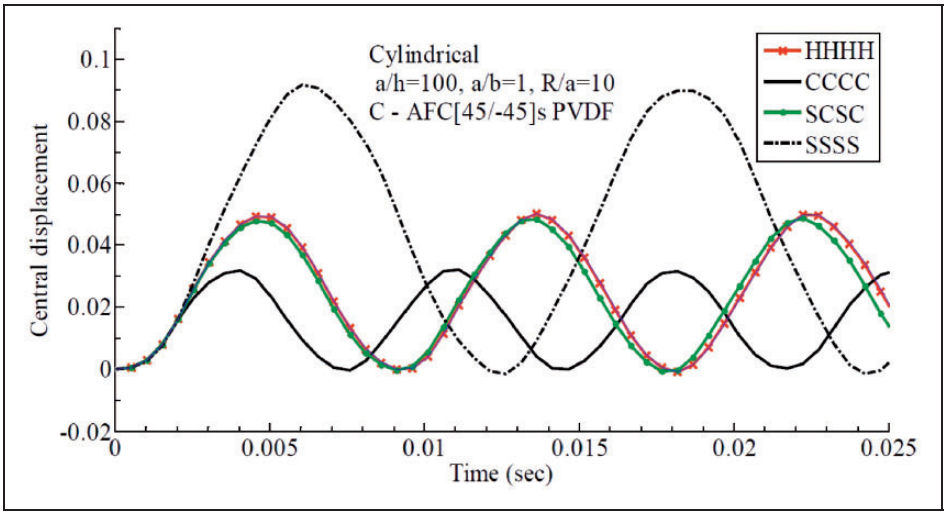

Figure 16. Effect of different boundary conditions on nonlinear transient response of cylindrical composite shell panel.

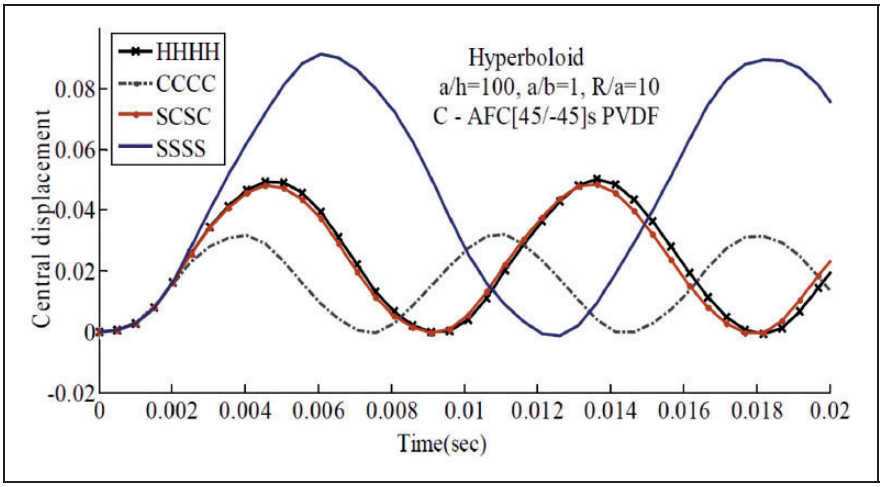

Figure 17. Effect of different boundary conditions on nonlinear transient response of hyperboloid composite shell panel.

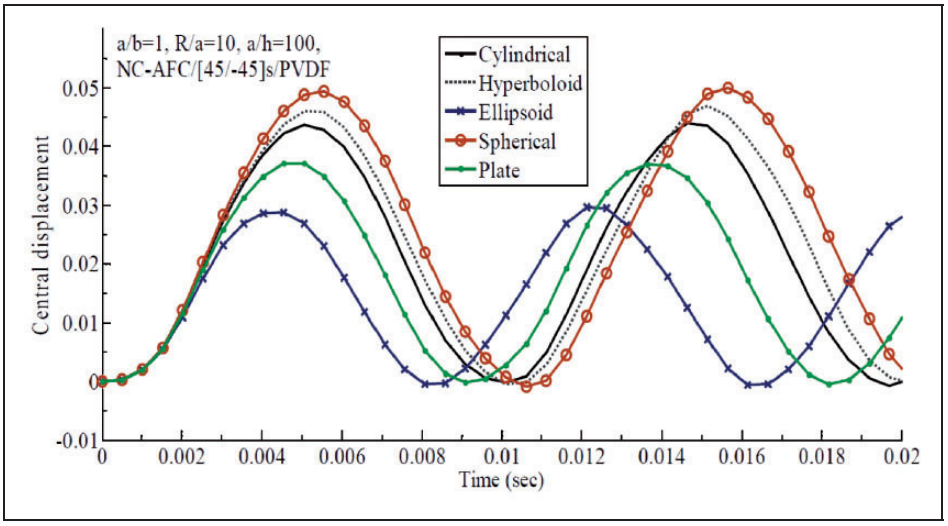

Figure 18. Effect of different shell forms on nonlinear transient response of angle-ply for NC-arrangement.

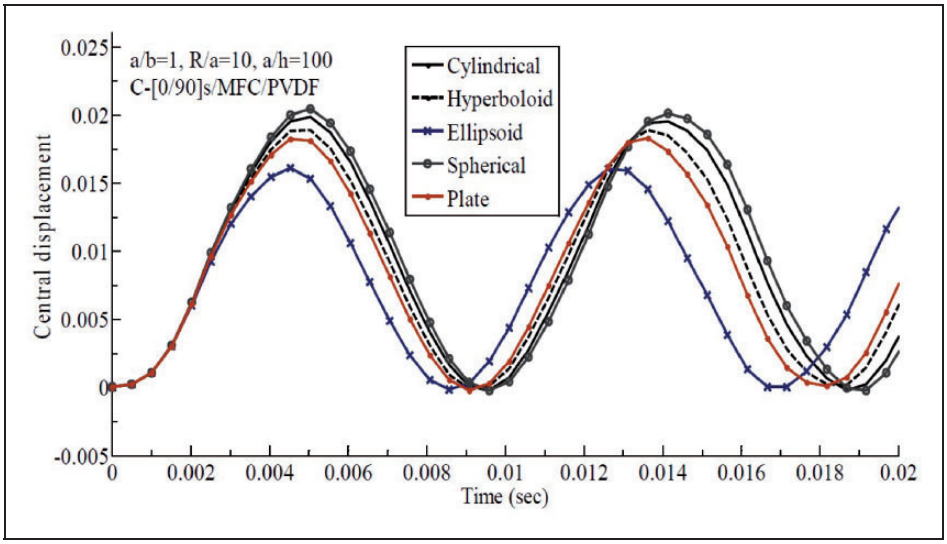

Figure 19. Effect of different shell forms on nonlinear transient response of cross-ply C-arrangement.

are computed for the various types of support conditions (SSSS/HHHH/CCCC/SCSC) and shown in Figures 16 and 17 for the cylindrical and hyperboloid type of shell panels, respectively. It is observed that as the degree of constraints increases the magnitude of nonlinear transient deformation decreases irrespective of the shell geometrical configurations i.e. in case of SSSS the responses are highest and in case of CCCC it is the least. It is also noted that the cylindrical panel shows higher magnitude of dynamic responses as compared to the hyperboloid shell panels.

Effect of different shell forms on nonlinear transient responses of cross-ply and angle-ply sensor/actuator arrangements. Shell forms or shell geometrical configurations are defined on the basis of the principal radii of curvatures (R_x and R_y) and the twist radius (R_{xy}). As the present study is confined to only the shallow shells the twist radius is infinite (∞) in all the shell forms. Therefore, the nonlinear dynamic responses of different shell form namely, cylindrical, hyperboloid, ellipsoid, spherical and flat panels are computed and presented in this section. Figures 18 and 19 show the nonlinear transient deflection values for the non-collocated angle-ply (NC-AFC/[45°/−45°]s/PVDF) and the collocated cross-ply (C-[0°/90°]s/MFC/PVDF) configurations, respectively. It is seen that the NC-configuration suffers with the higher nonlinear dynamic deformation as compared to the C-configuration. Thus, it can be inferred that the later one has the better control ability for such high amplitude responses. In addition to that the influence of the placement of piezoelectric sensor and actuator on the nonlinear transient responses of the smart composite shell panels is clearly evident from the figures.

Conclusion

The geometrically nonlinear transient bending responses of the curved piezoelectric composite shell panel structure computed numerically using a novel higher-order nonlinear mathematical model including Green-Lagrange nonlinear strain field. The coupled electromechanical formulation is developed in association with the FEM. The linear and nonlinear dynamic deflections are computed using Newmark's time integration algorithm (constant average-acceleration method) including the direct iterative method. The linear and nonlinear dynamic responses obtained using the present nonlinear model are compared with published results to demonstrate the accuracy. Additionally, an experimental validation for the active suppression of the dynamic responses of the PZT bonded composite plate verifies to access the robustness and inevitability of the presently developed higher-order nonlinear model. Further, the effect of geometrical parameters like curvature ratio (R/a), thickness ratio (a/h) and aspect ratio (a/b) and the boundary conditions on the nonlinear dynamic responses of the single/doubly curved piezoelectric bonded composite shell panels for the collocated and non-collocated types of sensor and the actuator arrangements are investigated. It is observed that the spherical panels reveal the highest amplitude of dynamic responses whereas the ellipsoid panels show the lowest one irrespective of the lamination scheme and the sensor/actuator arrangements. It is interesting to note that the non-collocated types of sensor or actuator arrangement show the higher magnitude of nonlinear dynamic responses in comparison to the collocated arrangement irrespective of shell forms and the other geometrical parameters. Thus, it can be concluded that the collocated arrangement is more capable of controlling the nonlinear dynamic responses in comparison to the non-collocated arrangement.

Declaration of Conflicting Interests

The author(s) declared no potential conflicts of interest with respect to the research, authorship, and/or publication of this article.

Funding

The author(s) disclosed receipt of the following financial support for the research, authorship, and/or publication of this article: This work is under the project sanctioned by the Department of Science and Technology (DST) through grant SERB/F/1765/2013-2014 Dated: 21/06/2013.

ORCID iD

Chetan K Hirwani http://orcid.org/0000-0003-4291-4575
Subrata K Panda http://orcid.org/0000-0001-8841-7449
Trupti R Mahapatra http://orcid.org/0000-0001-7567-4323
Kulmani Mehar http://orcid.org/0000-0001-5088-6813

References

1. Sahoo SS, Panda SK and Mahapatra TR. Static, free vibration and transient response of laminated composite curved shallow panel – an experimental approach. *Eur J Mech A Solids* 2016; 59: 95–113.
2. Hirwani CK, Patil RK, Panda SK, et al. Experimental and numerical analysis of free vibration of delaminated curved panel. *Aerosp Sci Technol* 2016; 54; 353–370.
3. Mahapatra TR, Kar VR and Panda SK. Large amplitude bending behaviour of laminated composite curved panels. *Eng Comput* 2016; 33: 116–138.
4. Lam KY, Peng QX, Liu RG, et al. A finite-element model for piezoelectric composite laminates. *Smart Mater Struct* 1997; 6: 583–591.
5. Liao L and Yu W. An electromechanical Reissner-Mindlin model for laminated piezoelectric plates. *Compos Struct* 2009; 88:94–402.
6. Reddy JN. On laminated composite plates with integrated sensors and actuators. *Eng Struct* 1999; 21: 568–593.
7. Lee CK. Theory of laminated piezoelectric plates for the design of distributed sensors/actuators. Part I: governing equations and reciprocal relationships. *J Acoust Soc Am* 1990; 87: 1144–1158.
8. Pai PF, Nayfeh ALIH, Oh K, et al. A refined nonlinear model of composite plates with integrated piezoelectric actuators and sensors. *Int J Solids Struct* 1993; 30: 1603–1630.
9. Mitchell JA and Reddy JN. A refined hybrid plate theory for composite laminates with piezoelectric laminae. *Int J Solids Struct* 1995; 32: 2345–2367.
10. Lee YY and Ng C-F. Vibration control of composite plates under random loading using piezoelectric material. *Proc IMechE, Part C: J Mechanical Engineering Science* 2000; 214: 9–25.
11. Sunar M and Al-Bedoor BO. Vibration measurement of a cantilever beam using root embedded piezoceramic sensor. *Proc IMechE, Part C: J Mechanical Engineering Science* 2008; 222: 147–161.
12. Kerur SB and Ghosh A. Active control of geometrically non-linear transient response of smart laminated composite plate integrated with AFC actuator and PVDF sensor. *J Intell Mater Syst Struct* 2011; 22: 1149–1160.
13. Shiyekar SM and Kant T. Higher order shear deformation effects on analysis of laminates with piezoelectric fibre reinforced composite actuators. *Compos Struct* 2011; 93: 3252–3261.
14. Mateescu D, Han Y and Misra A. Dynamics and vibrations of structures with bonded piezoelectric strips subjected to mechanical and unsteady aerodynamic loads. *Proc IMechE, Part C: J Mechanical Engineering Science* 2008; 225: 625–638.
15. Kumar RS and Ray MC. Active control of geometrically nonlinear vibrations of doubly curved smart sandwich shells using 1 – 3 piezoelectric composites. *Compos Struct* 2013; 105: 173–187.
16. Huang X and Shen H. Nonlinear free and forced vibration of simply supported shear deformable laminated plates with piezoelectric actuators. *Int J Mech Sci* 2005; 47: 187–208.
17. Shahraeeni M, Shakeri R and Mohammad S. An analytical solution for free and forced vibration of a piezoelectric laminated plate coupled with an acoustic enclosure. *Comput Math Appl* 2015; 69: 329–1341.
18. Jiang H, Liang L, Ma L, et al. An analytical solution of three-dimensional steady thermodynamic analysis for a piezoelectric laminated plate using refined plate theory. *Compos Struct* 2017; 162: 194–209.
19. Phung-van P, De Lorenzis L, Thai CH, et al. Analysis of laminated composite plates integrated with piezoelectric sensors and actuators using higher-order shear deformation theory and isogeometric finite elements. *Comput Mater Sci* 2015; 96: 495–505.
20. Phung-van P, Nguyen LB, Tran LV, et al. An efficient computational approach for control of nonlinear transient responses of smart piezoelectric composite plates. *Int J Non Linear Mech* 2015; 76: 190–202.
21. Robaldo A, Carrera E and Benjeddou A. A unified formulation for finite element analysis of piezoelectric adaptive plates. *Comp Struct* 2006; 84: 1494–1505.
22. Carrera E and Boscolo M. Classical and mixed finite elements for static and dynamic analysis of piezoelectric plates. *Int J Numer Meth Eng* 2007; 70: 1135–1181.
23. Carrera E and Robaldo A. Hierarchic finite elements based on a unified formulation for the static analysis of shear actuated multilayered piezoelectric plates. *Multidiscip Model Mater Struct* 2010; 6: 45–77.
24. Carrera E and Valvano S. Analysis of laminated composite structures with embedded piezoelectric sheets by variable kinematic shell elements. *J Intel Mater Sys Struct* 2017; 28: 2959–2987.
25. Kulikov GM, Plotnikova SV and Carrera E. Hybrid-mixed solid-shell element for stress analysis of laminated piezoelectric shells through higher-order theories. *Anal Model Adv Struct Smart Syst* 2018; 81: 45–68.
26. Ray MC and Sachade HM. Exact solutions for the functionally graded plates integrated with a layer of piezoelectric fiber-reinforced composite. *Am Soc Mech Eng* 2006; 73: 622–632.
27. Qing G, Xu J, Li P, et al. A new efficient numerical method and the dynamic analysis of composite laminates with piezoelectric layers. *Compos Struct* 2007; 78: 457–467.
28. Shen H and Yang D. Nonlinear vibration of anisotropic laminated cylindrical shells with piezoelectric fiber reinforced composite actuators. *Ocean Eng* 2014; 80: 36–49.
29. Saviz M. Dynamic analysis of a laminated cylindrical shell with piezoelectric layer and clamped boundary condition. *Finite Elem Anal Des* 2015; 104: 1–15.
30. Singh VK and Panda SK. Nonlinear free vibration analysis of single/doubly curved composite shallow shell panels. *Thin Walled Struct* 2014; 85: 341–349.

31. Benjeddou A, Deu JF and Letombe S. Free vibrations of simply-supported piezoelectric adaptive plates: an exact sandwich formulation. *Thin Walled Struct* 2002; 40: 573–593.
32. Singh VK, Mahapatra TR and Panda SK. Nonlinear flexural analysis of single/doubly curved smart composite shell panels integrated with PFRC actuator. *Eur J Mech A/Solids* 2016; 60: 300–314.
33. Reddy JN. *Mechanics of laminated composite plates and shells*. Florida: CRC Press, 2004.
34. Reddy JN. *An introduction to nonlinear finite element analysis*. New York: Oxford University Press, 2005.
35. Tzou HS and Tseng CI. Distributed piezoelectric sensor/actuator design for dynamic measurement/control of distributed parameter systems: a piezoelectric finite element approach. *J Sound Vib* 1990; 138: 17–34.
36. Chen J, Daw DJ and Wang S. Nonlinear transient analysis of rectangular composite laminated plates. *Compos Struct* 2000; 49: 129–139.
37. Kundu CK and Sinha PK. Nonlinear transient analysis of laminated composite shells. *J Reinf Plast Compos* 2006; 25: 1129–1147.
38. Kurtaran H. Geometrically nonlinear transient analysis of moderately thick laminated composite shallow shells with generalized differential quadrature method. *Compos Struct* 2015; 125: 605–614.

Appendix

Notation

a, b and h	length, width and thickness of the shell panel
a/b	aspect ratios
a/h	thickness ratios
$[B_l]$ and $[B_{nl}]$	linear and nonlinear strain-displacement matrix
d, d_0	global and mid-plane displacement vectors
$[K_d], [K_{d\phi}]$ $[K_{\phi d}], [K_{\phi\phi}]$	linear elastic, coupled electro-elastic and electric stiffness matrices
$[K_L]$	linear stiffness matrix
$[K_{NL}]$	geometric stiffness matrix
R/a	curvature ratios
R_x, R_y	principal radii of curvatures of shell panel
u, v and w	displacements in x, y and z direction respectively
x, y, z	cartesian coordinate axes
$\{\varepsilon\}$	strain tensor
$\{\varepsilon_l\}$, $\{\varepsilon_{nl}\}$	linear and nonlinear strain tensors
ϕ	electric potential
ψ_x, ψ_y, λ_x, λ_y	higher order terms of Taylor series expansion
$\{\sigma\}$	stress tensor
θ_x, θ_y	the rotations with respect to y and x direction
θ_z	thickness stretching term or transverse extension

Appendix 1

Mid-plane linear $\{\overline{\varepsilon_l}\}$ and nonlinear $\{\overline{\varepsilon_{nl}}\}$ strain terms

Individual terms of linear mid-plane strain matrix of equation (6)

$$\varepsilon_x^0 = u_{,x}\ \varepsilon_y^0 = v_{,y}\ \varepsilon_z^0 = w_{,z},$$

$$\varepsilon_{yz}^0 = \theta_y + w_{,y},\ \varepsilon_{xz}^0 = \theta_x + w_{,x},\ \varepsilon_{xy}^0 = u_{,y} + v_{,x},\ k_x^1 = \theta_{x,x},$$
$$k_x^2 = \psi_{x,x},\ k_x^3 = \lambda_{x,x},\ k_y^1 = \theta_{y,y},\ k_y^2 = \psi_{y,y},\ k_y^3 = \lambda_{y,y},$$
$$k_{yz}^1 = \theta_{z,y} + 2\psi_y,\ k_{yz}^2 = 3\lambda_y - \psi_y/R_y,\ k_{yz}^3 = -\lambda_y/R_y,$$
$$k_{xz}^1 = 2\phi_x + \theta_{z,x},\ k_{xz}^2 = 3\lambda_x - \psi_x/R_x,\ k_{xz}^3 = -\lambda_x/R_x,$$
$$k_{xy}^1 = \theta_{y,x} + \theta_{x,y},\ k_{xy}^2 = \psi_{x,y} + \psi_{y,x},\ k_{xy}^3 = \lambda_{x,y} + \lambda_{y,x}$$

Additionally, the combined terms are provided below

$$u_{,x} = \partial u_0/\partial x + w_0/R_x,\ u_{,y} = \partial u_0/\partial y + w_0/R_{xy},$$
$$v_{,x} = \partial v_0/\partial x + w_0/R_{xy},\ v_{,y} = \partial v_0/\partial y + w_0/R_y,$$
$$w_{,x} = \partial w_0/\partial x - u_0/R_x,\ w_{,y} = \partial w_0/\partial y - v_0/R_y,$$
$$w_{,z} = \partial w_0/\partial z,\ \theta_{x,x}^* = \partial\theta_x/\partial x + \theta_z/R_x,\ \psi_{x,x} = \partial\psi_x/\partial x,$$
$$\psi_{x,y} = \partial\psi_x/\partial y,\ \psi_{y,x} = \partial\psi_y/\partial x,\ \psi_{y,y} = \partial\psi_y/\partial y,$$
$$\lambda_{x,x} = \partial\lambda_x/\partial x,\ \lambda_{y,x} = \partial\lambda_y/\partial x,\ \lambda_{y,y} = \partial\lambda_y/\partial x$$

Individual terms in nonlinear mid-plane strain matrix of equation (7)

$$\varepsilon_x^{nl0} = 1/2\left[(u_{,x})^2 + (v_{,x})^2 + (w_{,x})^2\right],$$
$$\varepsilon_y^{nl0} = 1/2\left[(u_{,y})^2 + (v_{,y})^2 + (w_{,y})^2\right],$$
$$\varepsilon_z^{nl0} = 1/2\left[(\theta_x)^2 + (\theta_y)^2 + (\theta_z)^2\right],$$
$$\varepsilon_{yz}^{nl0} = \theta_x u_{,y} + \theta_y v_{,y} + \theta_z w_{,y},\ \varepsilon_{xz}^{nl0} = \theta_x u_{,x} + \theta_y v_{,x} + \theta_z w_{,x},$$
$$\varepsilon_{xy}^{nl0} = u_{,x}u_{,y} + v_{,x}v_{,y} + w_{,x}w_{,y},\ k_x^{nl1} = u_{,x}\theta_{x,x} + v_{,x}\theta_{y,x}$$
$$+ w_{,x}\theta_{z,x} + (\theta_z/R_x)u_{,x} + (\theta_z/R_{xy})v_{,x} - (\theta_x/R_x)w_{,x}$$
$$k_x^{nl2} = (\theta_{x,x})^2 + (\theta_{y,x})^2 + (\theta_{z,x})^2 + u_{,x}\psi_{x,x} + v_{,x}\psi_{y,x}$$
$$+ (\theta_z/R_x)u_{,x} + (\theta_z/R_{xy})v_{,x} - (\theta_x/R_x)w_{,x}$$
$$k_x^{nl3} = \lambda_{x,x}u_{,x} + \lambda_{y,x}u_{,x} - w_{,x}\lambda_x/R_x + \psi_{x,x}\theta_{x,x}^* + \psi_{y,x}\theta_{y,x}^*$$
$$k_x^{nl4} = \psi_{x,x}\theta_{x,x}^* + \psi_{y,x}\theta_{y,x}^* + \lambda_{x,x}u_{,x} + \lambda_{y,x}u_{,x}$$
$$- w_{,x}\lambda_x/R_x + (\theta_z/R_{xy})v_{,x} - (\theta_x/R_x)w_{,x}$$
$$k_x^{nl5} = u_{,x}\psi_{x,x} + v_{,x}\psi_{y,x} + (\theta_z/R_x)u_{,x} + (\theta_z/R_{xy})v_{,x}$$
$$- (\theta_x/R_x)w_{,x} + \psi_{x,x}\theta_{x,x}^* + \psi_{y,x}\theta_{y,x}^*$$
$$k_x^{nl6} = (\lambda_{x,x})^2 + (\lambda_{y,x})^2 + (\lambda_x/R_x)^2;$$
$$k_y^{nl1} = \lambda_{x,x}u_{,x} + \lambda_{y,x}u_{,x} + u_{,x}\psi_{x,x} + u_{,x}\psi_{x,x}$$
$$k_y^{nl2} = (\theta_{x,x})^2 + (\theta_{y,x})^2 + (\theta_{z,x})^2 + u_{,x}\psi_{x,x}$$
$$+ v_{,x}\psi_{y,x} + (\theta_z/R_x)u_{,x}$$

$$k_{y}^{nl4} = u_{,x}\theta_{x,x} + v_{,x}\theta_{y,x} + w_{,x}\theta_{z,x} + (\theta_z/R_x)u_{,x} + \left(\theta_z/R_{xy}\right)v_{,x} - (\theta_x/R_x)w_{,x}$$

$$k_{xy}^{nl2} = \lambda_{x,x}u_{,x} + \lambda_{y,x}u_{,x} - w_{,x}\lambda_x/R_x + \psi_{x,x}\theta^{*}_{x,x}\backslash + \psi_{y,x}\theta^{*}_{y,x}$$

$$k_{xy}^{nl3} = u_{,x}\theta_{x,x} + v_{,x}\theta_{y,x} + w_{,x}\theta_{z,x} + (\theta_z/R_x)u_{,x} + \left(\theta_z/R_{xy}\right)v_{,x} - (\theta_x/R_x)w_{,x}$$

$$k_{xy}^{nl4} = \lambda_{x,x}u_{,x} + \lambda_{y,x}u_{,x} - w_{,x}\lambda_x/R_x + \psi_{x,x}\theta^{*}_{x,x} + \lambda_{x,x}u_{,x} + \lambda_{y,x}u_{,x} + u_{,x}\psi_{x,x} + u_{,x}\psi_{x,x}$$

$$k_{xy}^{nl5} = u_{,x}\psi_{x,x} + u_{,x}\psi_{x,x} - w_{,x}\lambda_x/R_x + \psi_{x,x}\theta^{*}_{x,x} + \lambda_{x,x}u_{,x} + \lambda_{y,x}u_{,x} + u_{,x}\psi_{x,x} + u_{,x}\psi_{x,x}$$

$$k_{xy}^{nl6} = \lambda_x\lambda_y/R_xR_y + \lambda_{x,x}u_{,x} + \lambda_{y,x}u_{,x}$$